Supporting Information for:

Transport among protocells via tunneling nanotubes

Ingrid Jin Schanke[1†], Lin Xue[1†], Karolina Spustova[1], Irep Gözen[1,2*]

[1]Centre for Molecular Medicine Norway, Faculty of Medicine, University of Oslo, 0318 Oslo, Norway
[2]Department of Chemistry, Faculty of Mathematics and Natural Sciences, University of Oslo, 0315 Oslo, Norway

[†]These authors contributed equally to this work.

*To whom correspondence should be addressed. Email: irep@uio.no

Table of Contents

S1. Encapsulation of cargo molecules

Three different fluorescent cargo molecules with varying molecular weights were introduced to the protocell-nanotube networks (PNNs) using an open-space microfluidic pipette[1, 2]: a fluorescent dye (ATTO 488) (**Fig. S1a-b**), RNA (**Fig. S1c-d**) and DNA (**Fig. S1e-f**). Panels **a**,**c** and **e**, represent the part of the experiment during which the fluorescently labeled cargo molecules are continuously exposed to a region on the PNNs. Panels **b**,**d** and **f** shows the networks after ~4 min of exposure.

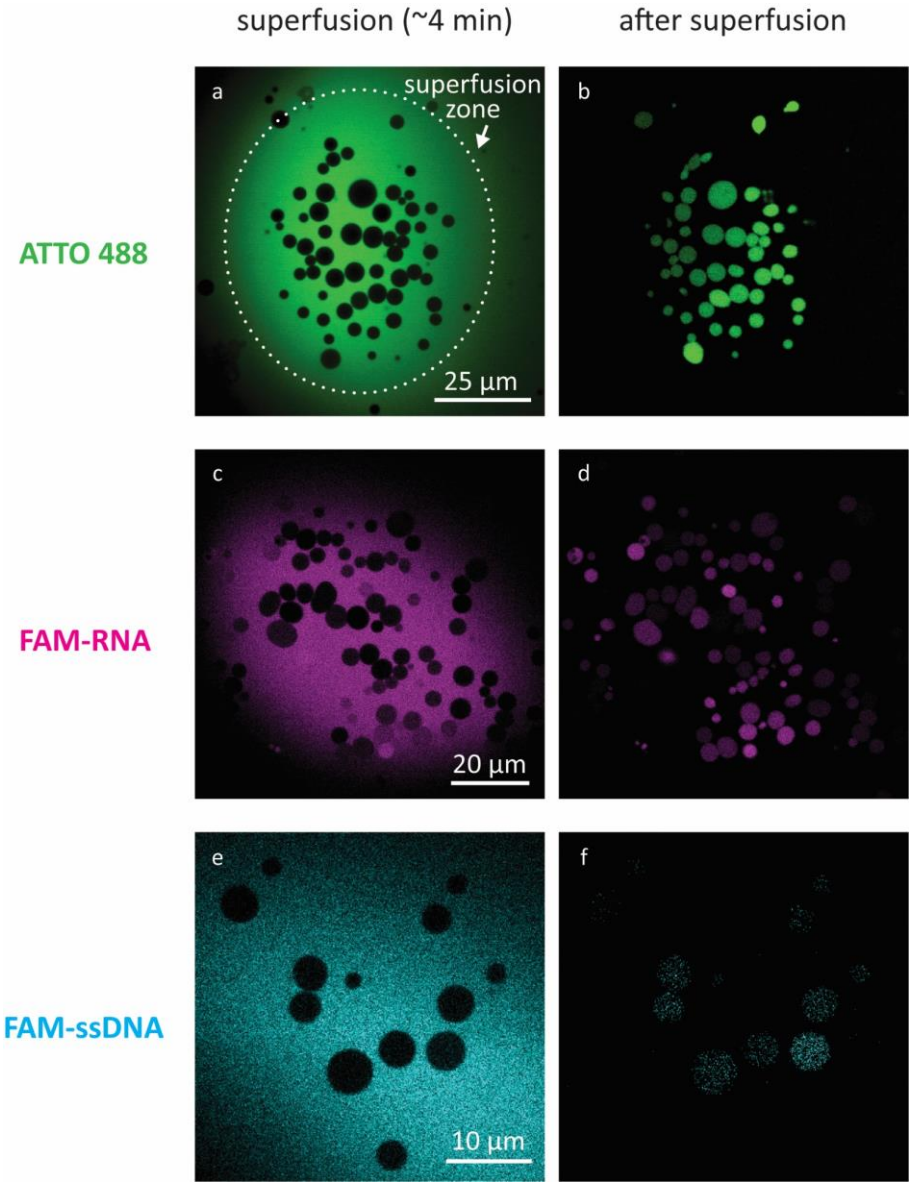

Figure S1. Encapsulation of different cargo molecules. **a, c, e**) Confocal micrographs ~4 min into the superfusion, and **b, d, f**) right after superfusion is terminated. (**a-b**) ATTO 488, (**c-d**) FAM-RNA, (**e-f**) FAM-ssDNA.

S2. FRAP of an isolated vesicle (control)

We performed a control FRAP experiment on an isolated, surface-adhered giant unilamellar vesicle (GUV) containing ATTO 488 (**Fig. S2a-b**). Upon photobleaching, no recovery was observed (**Fig. S2c-d**). This result confirms necessity of a nanotubular connection for recovery of the fluorescence intensity of a lipid compartment in PNNs.

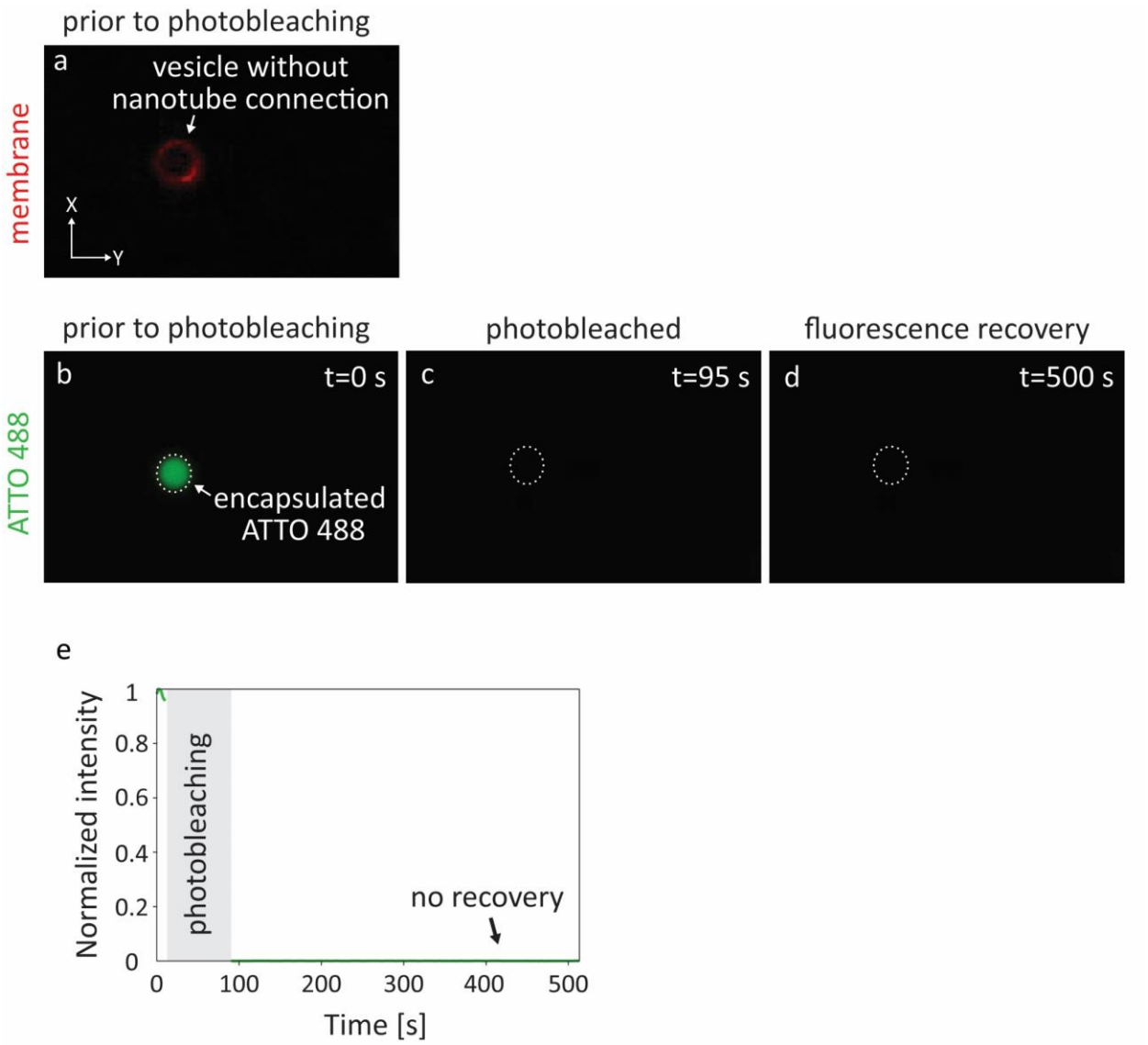

Figure S2. FRAP of an isolated GUV on a solid substrate. (**a-b**) Confocal micrograph of an isolated GUV, encapsulating ATTO 488. (**a**) shows the membrane fluorescence, and (**b**) the fluorescence of the internalized dye, ATTO 488. Photobleached GUV (**c-d**). (**e**) FRAP curve corresponding to (**b-d**). The diameter of the vesicle is 4 μm.

S3. FRAP experiments

Confocal microscopy time series corresponding to the plots shown in **Fig. 3** of the main manuscript. Several FRAP experiments were performed for each cargo molecule ATTO 488 (**Fig. S3**), RNA (**Fig. S4**) and DNA (**Fig. S5**). Each experiment is labeled with the capital letters matching the labels of the plots in **Fig. 3a,h,l**.

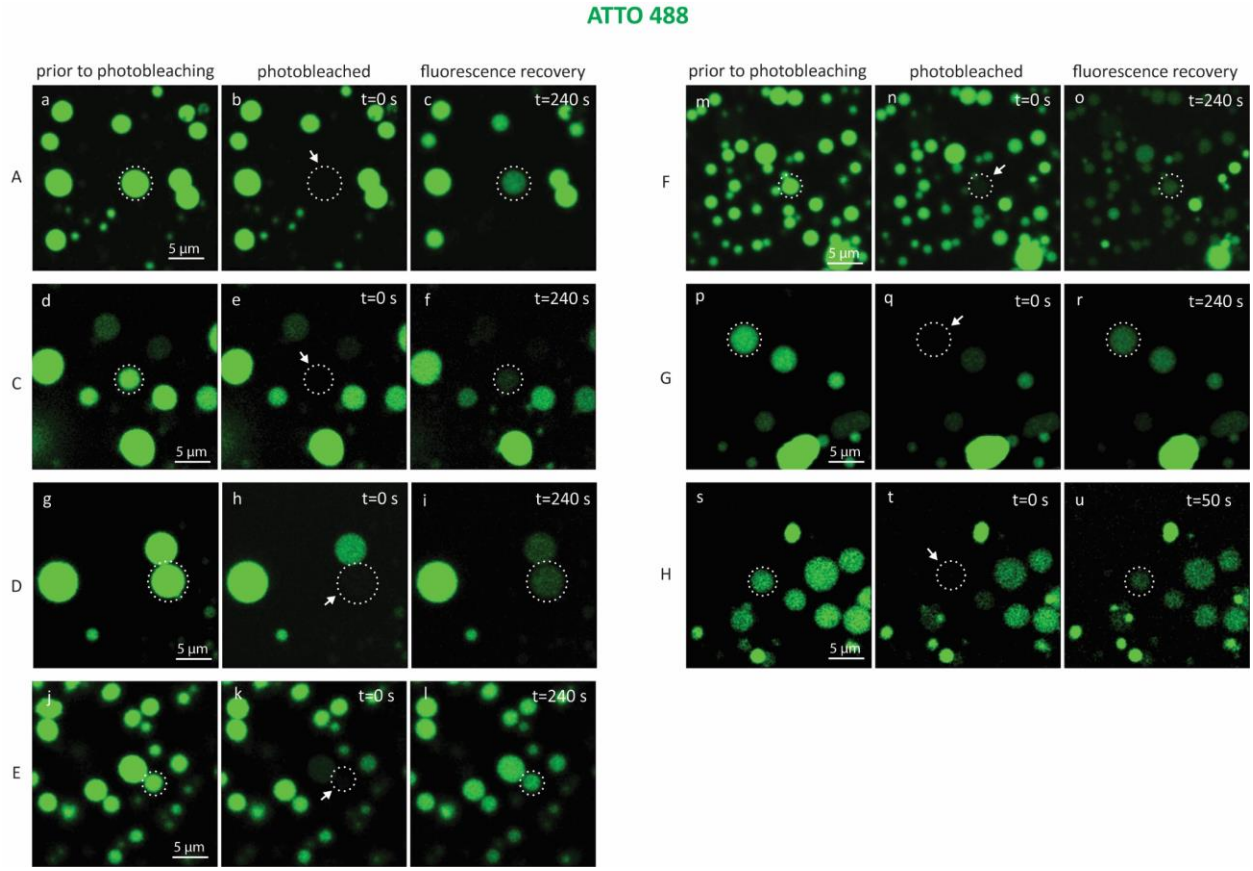

Figure S3. Confocal micrographs showing before, during and after photobleaching of compartments encapsulating **ATTO 488** in different experiments: A (**a-c**), C–H (**d-u**). Each set of micrographs show a model protocell targeted for photobleaching (encircled in dotted lines). Three time points in each experiment represent: prior to photobleaching, during photobleaching (arrows) and during fluorescence recovery.

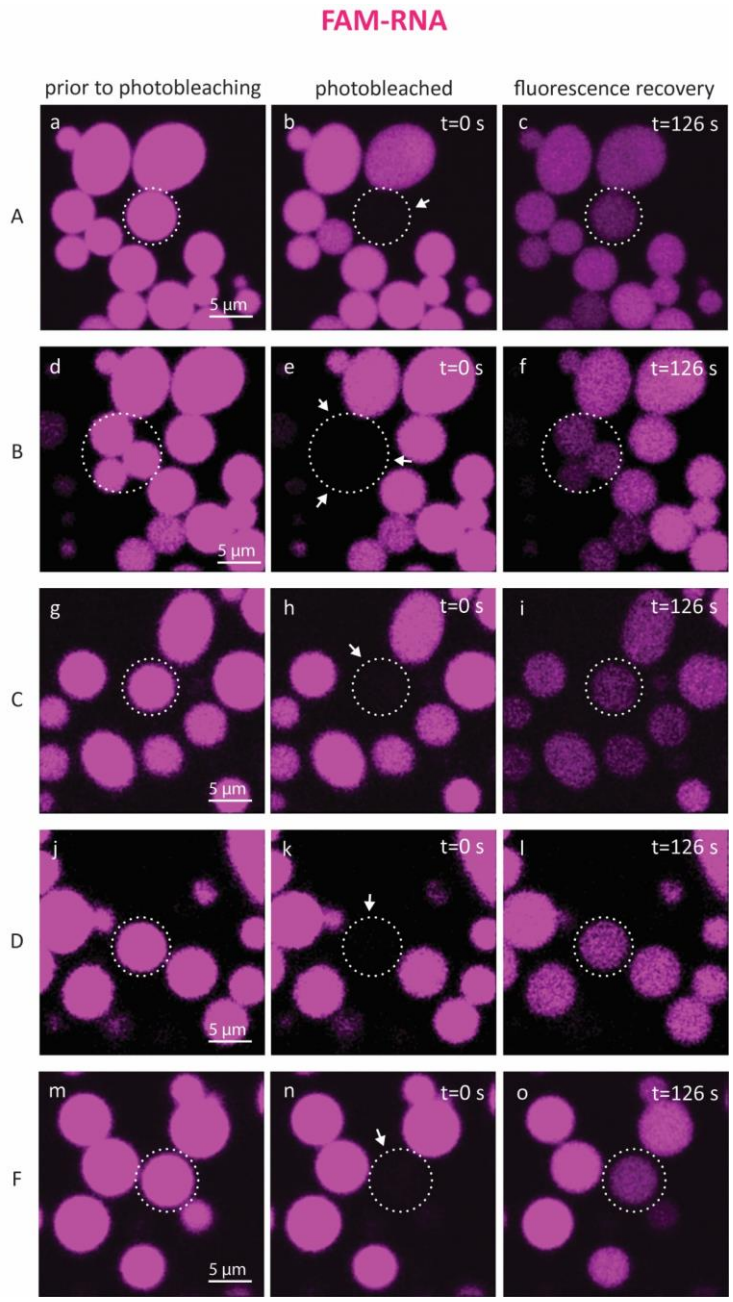

Figure S4. Confocal micrographs showing before, during and after photobleaching of compartments encapsulating **RNA** in different experiments: A-F (**a-o**). Each set of micrographs show a model protocell targeted for photobleaching (encircled in dotted lines). Three time points in each experiment represent: prior to photobleaching, during photobleaching (arrows) and during fluorescence recovery.

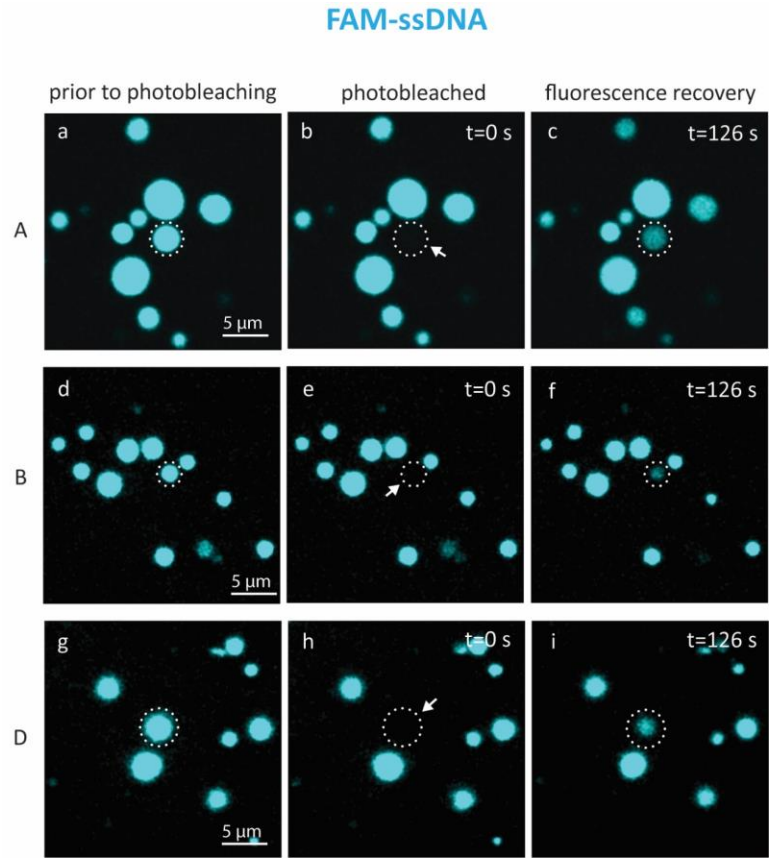

Figure S5. Confocal micrographs showing before, during and after photobleaching of compartments encapsulating **DNA** in different experiments: A-D (**a-i**). Each set of micrographs show a model protocell targeted for photobleaching (encircled in dotted lines). Three time points in each experiment represent: prior to photobleaching, during photobleaching (arrows) and during fluorescence recovery.

S4. Fluorescence recovery in a two-compartment system

A FRAP experiment followed by the transport of ATTO 488 between two adjacent protocells has been presented in **Fig. S6a-c** (same as **Fig. S3d**). **Fig. S6d** shows the fluorescence intensity of the donor (yellow plot) and acceptor (green plot) protocell, over time. The dashed line is the theoretical fit based on a two-compartment model[3] (**Fig. 4**), which overlaps with the fluorescence recovery (green plot). The high fluorescence intensity of the leftmost protocell in **Fig. S6c** maintains during several minutes, indicating that it has no open nanotubular connection to protocell 1 or 2, and is not a contributing donor compartment (**Fig. S6a**).

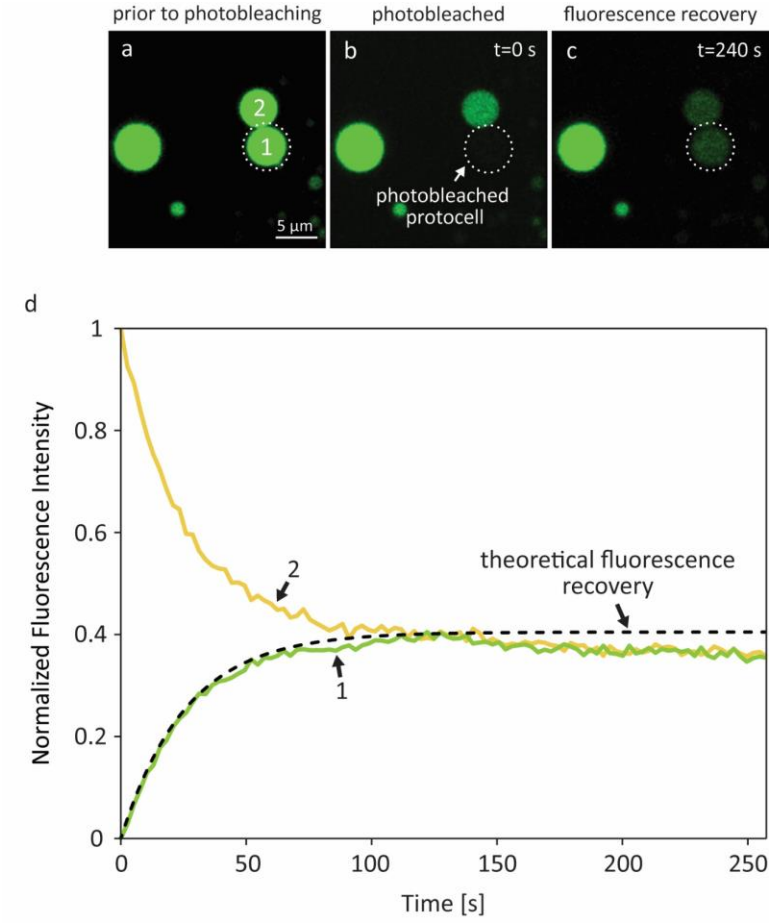

Figure S6. Fluorescence intensity of a two-compartment system after photobleaching of one of the compartments. (**a-c**) Protocell 1 (encircled in dotted line) is photobleached. (**d**) Fluorescence intensity of the donor (yellow plot) and acceptor (green plot) vesicle, over time.

After 100 s the fluorescence intensity of compartments #1 and #2 (**Fig. S6d**) reach an equilibrium at 40% of the initial concentration of the donor compartment (#2). If the

experimental system depicted in **Fig. S6** was free of dissipation factors[4] such as leakage or photobleaching, both protocells would reach 50% of the initial concentration, as predicted by analytical and numerical methods that describe diffusive transport of non-interacting particles in a two-vesicle system[5]. However, the total amount of fluorescence intensity of the two protocells in **Fig. S6** reaches approximately 80% after 100 s; 20% have been lost due to other factors than inter-vesicular transport.

The characteristic time of leakage from a single lipid vesicle, τ, can be used to calculate the permeability coefficient P of a solute through the vesicular membrane: $\tau = \frac{V}{SP}$ where V and S are the internal volume and surface area of the vesicle, respectively[6, 7]. This expression can be simplified as $= \frac{R}{3P}$, where R is the vesicle radius. The fluorescence intensity $I(t)$ inside a vesicle at a given time t is given as $I(t) = I_0 + (I_\infty - I_0)\left(1 - e^{-\frac{t}{\tau}}\right)$, where I_0 is the initial fluorescence intensity of the vesicle, i.e. before leakage, and I_∞ is the intensity after an infinite period[6, 7]. $I_0 = 1$ (100% at t=0 s in **Fig. S6**). After an infinite period, the cargo completely leaks out and is diluted in the ambient buffer, thus $I_\infty = 0$. This leads to $I(t) = e^{-\frac{t}{\tau}}$ and $P = \frac{-R \ln I(t)}{3t}$.

Assuming that a loss of 20% of the total intensity from a vesicle during 100 s is entirely due to leakage ($I(t) = 0.8$), where R =2.1 μm (Fig. S6), P can be determined as $0.156 \times 10^{-6} cm/s$. The permeability coefficient depends on various factors[8], e.g. membrane composition, lipid phase, chain length, sterol type. Permeability coefficients of different lipid membranes have been reported[9-12]. P across a DMPC:DPPC (50:50) bilayer was calculated as $0.2 \times 10^{-9} cm/s$ for ATP. P of fluorescein through GUVs composed of DPPC, DOPC and cholesterol (1:1:1) was determined as $19.4 \pm 1.8 \times 10^{-6}\ cm/s$ by Li et al. [12]. For vesicles with the same phospholipid composition as used in our work, P values for fluorescein and 10-base RNA taken up are $\sim 0.5 - 1.0 \times 10^{-6}\ cm/s$ [11], slightly higher than what we determine for ATTO 488 in the experiment related to **Fig. S6**. In summary, it is plausible that the 20% fluorescence loss over time could be due to leakage through the membrane, but we also take into account content loss from photobleaching. The latter is not a physical loss, but a reduction of signal from fluorescent species that are still within the container.

Fig. S7a shows the cross-section of the protocells in **Fig. S6a**. Despite their proximity, spontaneous fusion between the compartments is not likely, as energy input is required to create pores in initially isolated bilayers. Fusion in PNNs induced by external cues was previously observed, and characterized with a mathematical model[13]. It is expected that if the two compartments fuse at their equator, they will rapidly form a larger

compartment containing a stable circular pore (**Fig. S7b-d**). Maintaining a transient state over minutes (**Fig. S7c**) is not energetically favorable, therefore it is not likely that the compartments shown in **Fig. S6a/S7a**, are fused.

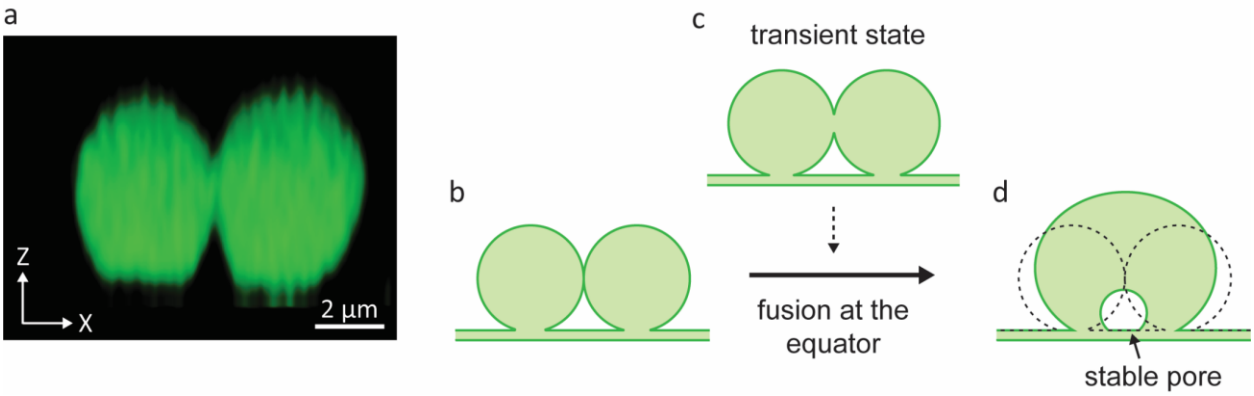

Figure S7. Possible steps of fusion of adjacent protocells**.** (**a**) Cross-section of the adjacent protocells in Fig. S6. (**b-d**) The possible steps of fusion between the compartments in PNNs, induced by external cues.

S5. Supporting Movie

Movie S1. Rapid formation of protocells during DNA exposure. Laser scanning confocal microscopy time series showing rapid formation and growth of protocells from the nanotube network during DNA exposure.

References

1. Ainla, A.; Jansson, E. T.; Stepanyants, N.; Orwar, O.; Jesorka, A., A Microfluidic Pipette for Single-Cell Pharmacology. *Anal. Chem* **2010,** *82* (11), 4529-4536.
2. Ainla, A.; Jeffries, G. D. M.; Brune, R.; Orwar, O.; Jesorka, A., A multifunctional pipette. *Lab Chip* **2012,** *12* (7), 1255-1261.
3. Dagdug, L.; Berezhkovskii, A. M.; Shvartsman, S. Y.; Weiss, G. H., Equilibration in two chambers connected by a capillary. *The Journal of chemical physics* **2003,** *119* (23), 12473-12478.
4. Sott, K.; Lobovkina, T.; Lizana, L.; Tokarz, M.; Bauer, B.; Konkoli, Z.; Orwar, O., Controlling Enzymatic Reactions by Geometry in a Biomimetic Nanoscale Network. *Nano Letters* **2006,** *6* (2), 209-214.
5. Lizana, L.; Konkoli, Z., Diffusive transport in networks built of containers and tubes. *Phys Rev E Stat Nonlin Soft Matter Phys* **2005,** *72* (2 Pt 2), 026305-026305.
6. Lawaczeck, R., On the permeability of water molecules across vesicular lipid bilayers. *The Journal of membrane biology* **1979,** *51* (3-4), 229-261.
7. Faure, C.; Nallet, F.; Roux, D.; Milner, S. T.; Gauffre, F.; Olea, D.; Lambert, O., Modeling Leakage Kinetics from Multilamellar Vesicles for Membrane Permeability Determination: Application to Glucose. *Biophys J* **2006,** *91* (12), 4340-4349.
8. Frallicciardi, J.; Melcr, J.; Siginou, P.; Marrink, S. J.; Poolman, B., Membrane thickness, lipid phase and sterol type are determining factors in the permeability of membranes to small solutes. *Nat Commun* **2022,** *13* (1), 1605-1605.

9. Sacerdote, M. G.; Szostak, J. W., Semipermeable Lipid Bilayers Exhibit Diastereoselectivity Favoring Ribose. *Proc Natl Acad Sci U S A* **2005,** *102* (17), 6004-6008.
10. Monnard, P.-A.; Deamer, D. W., Nutrient uptake by protocells: A liposome model system. *Orig Life Evol Biosph* **2001,** *31* (1-2), 147-155.
11. Poldsalu, I.; Koksal, E. S.; Gozen, I., Mixed fatty acid-phospholipid protocell networks. *Phys Chem Chem Phys* **2021,** *23* (47), 26948-26954.
12. Li, S.; Hu, P.; Malmstadt, N., Confocal Imaging to Quantify Passive Transport across Biomimetic Lipid Membranes. *Anal. Chem* **2010,** *82* (18), 7766-7771.
13. Köksal, E. S.; Liese, S.; Xue, L.; Ryskulov, R.; Viitala, L.; Carlson, A.; Gözen, I., Rapid Growth and Fusion of Protocells in Surface-Adhered Membrane Networks. *Small (Weinheim an der Bergstrasse, Germany)* **2020,** *16* (38), 2002529-n/a.